NANO LETTERS

2005
Vol. 5, No. 5
975−979

Versatile Visualization of Individual Single-Walled Carbon Nanotubes with Near-Infrared Fluorescence Microscopy

Dmitri A. Tsyboulski, Sergei M. Bachilo, and R. Bruce Weisman*

Department of Chemistry, Center for Biological and Environmental Nanotechnology, and Center for Nanoscale Science and Technology, Rice University, 6100 Main Street, Houston, Texas 77005

Received February 25, 2005

ABSTRACT

Fluorescence microscopy in the near-infrared between 950 and 1600 nm has been developed as a novel method to image and study single-walled carbon nanotubes (SWNTs) in a variety of environments. Intrinsic photoluminescence of disaggregated pristine SWNTs was excited by a diode laser and detected with a two-dimensional InGaAs photodiode array. Individual nanotubes were visualized with a spatial resolution of ca. 1 μm and characterized with polarization measurements and emission spectroscopy. Spatially resolved emission spectra allowed (*n*,*m*) identification of single nanotubes and revealed small environmentally induced spectral shifts between segments of long tubes. Nanotube motions in aqueous surfactant were visualized with a time resolution of 50 ms and used to estimate the diffusion coefficient.

Introduction. Single-walled carbon nanotubes (SWNTs) continue to attract intense research attention because of their unique electronic, mechanical, thermal, and optical properties.[1] The synthesis, processing, and study of nanotubes are guided by a number of powerful visualization and characterization methods that include scanning electron microscopy (SEM), scanning tunneling microscopy (STM), atomic force microscopy (AFM), and transmission electron microscopy (TEM). These microscopic methods can provide very high spatial resolutions that allow determinations of nanotube lengths and even diameters, but at the cost of experimental complexity, instrumentation expense, limited imaging speed, and restricted sample environments. Recently, optical methods with coarser spatial resolution have also been applied to image nanotubes through scanning resonant Raman microscopy, using both confocal and near-field approaches.[2−5]

Fluorescence microscopy offers yet another tool for nanotube observation and characterization. Several groups have reported the successful sidewall derivatization of nanotubes with fluorescent markers that make observation of single nanotubes possible using conventional fluorescent microscopes.[6−8] It is often preferable, however, to microscopically image the intrinsic near-infrared fluorescence of pristine semiconducting SWNTs.[9] The first benefit of this approach is that the precise diameter and chirality of a nanotube can be deduced from its near-infrared spectral emission signature because SWNT fluorescence wavelengths have been successfully assigned to specific (*n*,*m*) species.[10] In addition, the unusual near-infrared wavelengths of SWNT fluorescence provide high discrimination against background emission by other sample components. The absorption and emission transitions of SWNTs are strongly polarized along the tube axis, allowing determination of a nanotube's orientation through polarization measurements. Finally, the use of pristine nanotubes avoids the need for derivatization reactions and allows observation of intrinsic nanotube behavior unperturbed by chemical alterations. Although SWNTs exhibit low fluorescence quantum yields, several groups have reported microscopic spectral measurements on individual nanotubes.[11−15] Hartschuh et al. have also used a confocal scanning approach to construct near-infrared fluorescence images of smaller-diameter nanotubes that emit at wavelengths short enough to be observed with a silicon detector.[11] We describe here the use of a conventional far-field microscope coupled to a two-dimensional InGaAs photodiode array to conveniently visualize a wide range of individual pristine SWNTs in a variety of environments, including polymeric matrices and liquid media. The parallel, nonscanning detection advantage afforded by our method allows images with more than 80 000 pixels to be captured in as little as 50 ms, permitting the tracking of individual nanotube motions. In addition, the instrument is readily coupled to a spectrograph to provide spatially resolved emission spectra and (*n*,*m*) identification of individual nanotubes. Using spatially resolved spectroscopy, we have found subtle spectral variations between different regions of a single nanotube. This effect demonstrates the localized

* Corresponding author. E-mail: weisman@rice.edu

10.1021/nl050366f CCC: $30.25
Published on Web 04/15/2005

nature of SWNT excitons and the presence of environmentally induced inhomogeneous broadening within individual nanotubes.

Experimental Methods. Fluorescence microscopy was performed using a Nikon TE-2000 inverted microscope coupled via one of its output ports to an Indigo Alpha NIR InGaAs camera (320 × 256 pixels) that had been modified for reduced dark current backgrounds. Some images were obtained using a prototype OMA-V:2D liquid-nitrogen-cooled InGaAs camera from Roper Scientific. Samples were excited with an external 660 nm diode laser whose beam was focused by an aspheric lens ($f = 18.4$ mm) mounted on an XYZ translation stage. The excitation power at the sample was approximately 20 mW, and the excitation intensity could be varied from ca. 1 to 30 kW/cm^2. The polarization plane of the excitation laser was adjusted by rotation of a half-wave retardation plate. Nanotube emission was collected with a Nikon PlanApo 60×/1.4 oil-immersion objective. To selectively transmit the near-IR nanotube emission and block excitation light, we used a dichroic beam splitter in series with a dielectric long-pass filter having a cut wavelength of either 946 or 1125 nm. Single-frame acquisition times of 2 s were used with the Indigo camera. To measure spatially resolved emission spectra of objects in the microscope's observation field, a second output port of the Nikon TE-2000 was coupled to the input slit of a J-Y C140 spectrograph with a cryogenically cooled 512-element InGaAs array (Roper OMA-V) at its focal plane. The entrance slit gave a spectral band-pass of 3 nm. Its physical dimensions of 0.5 × 0.1 mm encompassed a 10 × 2 pixel region of the camera at 60× magnification. The spectrum of a nanotube could be easily measured by moving it to a specific position in the imaged field and then switching the microscope from its imaging port to the spectrograph port. Spectra were typically acquired by averaging 10 exposures of 20 s each.

HiPco SWNTs with diameters between 0.6 and 1.4 nm were obtained from the Rice Carbon Nanotechnology Laboratory. Aqueous suspensions of SWNTs in SDBS (sodium dodecylbenzenesulfonate) were prepared by ultrasonic dispersion and ultracentrifugation, as previously reported.[9,10] We prepared solid films of nanotubes by dissolving PVP (poly(vinylpyrrolidone), 40 000 average molecular weight) in DI water in amounts up to ca. 0.1 g/mL to yield moderately viscous solutions, and then adding aqueous SDBS suspensions of nanotubes in desired amounts. The resulting suspensions of nanotubes in SDBS and PVP (or in SDBS only) were spin-coated onto fused silica microscope slides and dried to obtain solid films containing separated nanotubes. To prepare liquid samples for microscopy, several microliters of aqueous SWNT suspensions were spread and sealed between a microscope slide and a cover slip.

Although as-grown HiPco samples generally contain a fraction of SWNTs with lengths of several micrometers, normal dispersion through vigorous ultrasonication appears to cut these longer nanotubes and leave only submicrometer species.[9,11] To achieve dispersion while preserving the long nanotubes, we added several micrograms of raw HiPco product into 10 mL of 1% SDBS/H_2O solution and applied

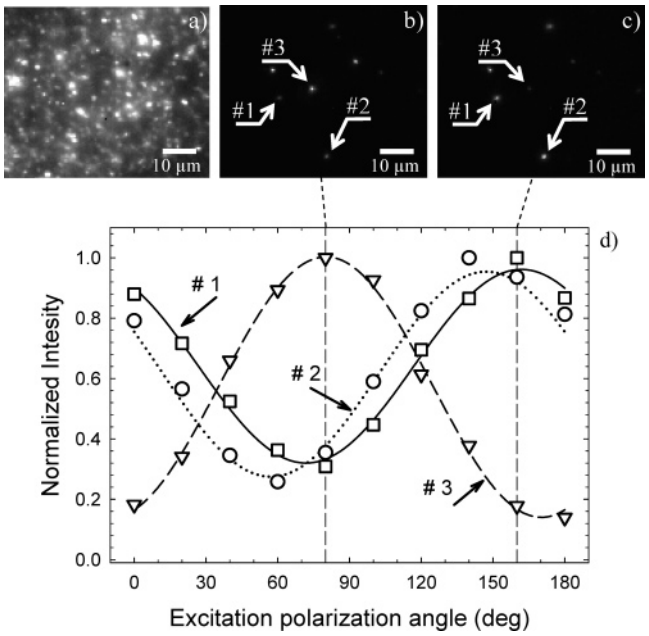

Figure 1. Near-IR fluorescence images of SWNT in PVP films at high (a) and low (b, c) concentrations. The excitation beam polarization angle was 80° in (b) and 160° in (c). The dependence of fluorescence intensity on polarization angle is plotted in frame (d) for the three labeled objects in images (b) and (c).

5 to 10 W of power to a small ultrasonic immersion probe for just 5 to 10 s. After this processing, the samples contain mainly submicrometer nanotubes with a small number of longer ones. Other workers have also reported the use of brief sonication to obtain dispersions containing long SWNTs.[16] Following the dispersion process, our samples were coarse-filtered to remove large residual nanotube aggregates, added to aqueous PVP solution, deposited onto a fused silica substrate, and dried.

Results and Discussion. Fluorescence from SWNT in solid films was readily imaged using the near-infrared microscope described above. Figure 1a shows many emission centers in the fluorescence image of a sample with relatively high SWNT concentration. Figure 1b is a similar image of a film that is much more dilute in nanotubes. Here the emitters appear sparse and isolated. The apparent diameter of individual emission features is approximately 1 μm, near the estimated optical resolution of our system. Although scanned confocal images have been reported previously in a study that used a Si CCD to capture fluorescence from the smallest diameter SWNTs (at wavelengths below ca. 1030 nm),[11] the InGaAs camera used here is sensitive from 900 to 1600 nm, allowing detection of a wide range of semiconducting nanotube species. The image in Figure 1c shows a different intensity pattern in the sample of Figure 1b when the excitation beam's polarization axis is rotated by 80°. (Note that the detection system has no polarization selection.) Variations in emission intensity with excitation polarization are plotted in Figure 1d for the three labeled points. All show a strong cos^2 dependence, as is consistent with individual SWNTs undergoing excitation of E_{22} van Hove transitions polarized along the tube axis. The differing angles of

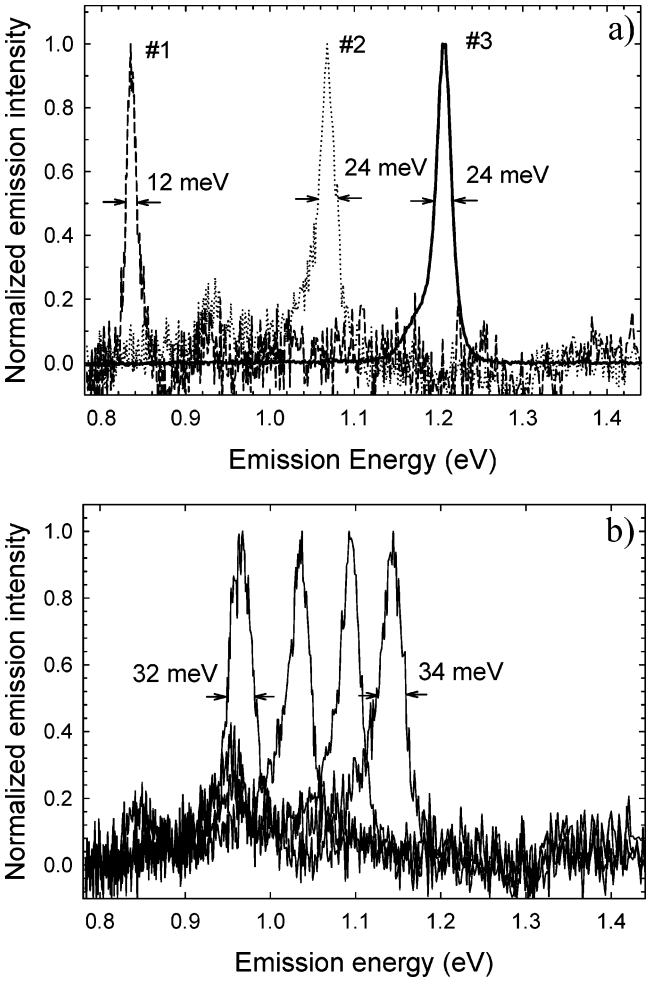

Figure 2. Emission spectra of selected individual nanotubes in dried aqueous SDBS (a) and PVP (b).

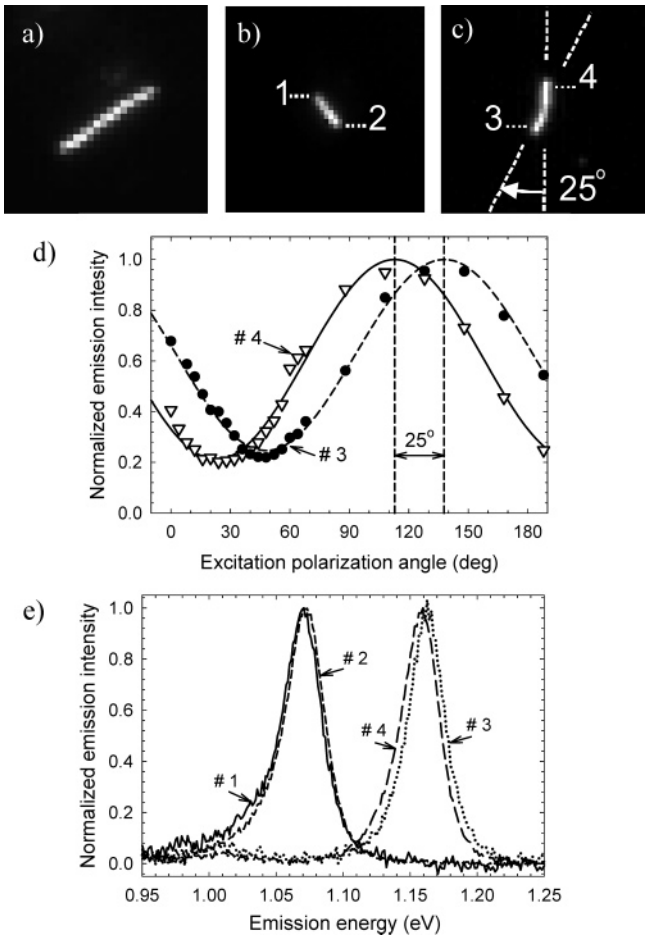

Figure 3. Near-infrared fluorescence images of single nanotubes recorded with magnifications of 60× (a), 90× (b), and 90× (c). Each image area is 15 × 15 μm. (d) Dependence of emission intensity on excitation polarization for the two ends of the nanotube in frame (c). (e) Spatially resolved emission spectra of the ends of the nanotubes in frames (b) and (c).

maximum intensity reveal the random azimuthal orientations of nanotubes in the sample.

To confirm the observation of individual nanotubes with near-IR microscopy, we recorded emission spectra of the three centers labeled in Figure 1b. As shown in Figure 2, each center gives a distinct, relatively narrow spectrum representing the E_{11} transition of a specific (*n*,*m*) SWNT. The observation of well-defined emission peaks and strong polarization effects indicates that each of these emitting centers is a single SWNT. Peak #3 arises from a (7,5) nanotube; peak #2 is assigned as an (8,6); and peak #1 is tentatively identified as (13,3). For larger diameter nanotubes that have E_{11} values below 1 eV (emission wavelengths greater than 1200 nm), the high spectral density can make (*n*,*m*) identification based on emission spectra ambiguous unless additional excitation wavelengths are available.

Many of the emission spectra observed for single nanotubes in dried SDBS show full-widths at half-maximum of approximately 24 meV (185 cm^{-1}). This value is consistent with the widths found in bulk samples in aqueous SDBS suspension. However, some individual nanotubes in dried SDBS show narrower emission widths of only ca. 12 meV (e.g., peak #1 in Figure 2a), which is similar to the 10 to 15 meV widths reported by Lefebvre et al. for individual air-suspended nanotubes at room temperature. In addition, our spectra of individual tubes in PVP films reveal broader emission line widths of 30 to 35 meV, as shown in Figure 2b. It appears then that much of the spectral width for typical nanotubes in condensed environments arises from inhomogeneous broadening within a single tube. This suggests the presence of multiple emission centers (fluorophore regions) along the tube axis with locally differing environments. It seems that energy migration processes between fluorophore regions may be related to the complex temperature-dependent spectra reported in a study of individual SWNTs at cryogenic temperatures.[15]

Further insights have been obtained by examining SWNTs that are long enough to be optically resolved in our fluorescence microscope. Using samples prepared with the mild sonication procedure described in Experimental Methods, we were able to observe clearly elongated fluorescence images, as shown in Figure 3. The objects imaged in frames a, b, and c are approximately 8, 3, and 4 μm long, respectively. To verify that these emitters are single nanotubes, we have measured spatially resolved polarization dependences (averaging data over 25 adjacent pixels) and emission spectra. Emitters that show linear images, such as

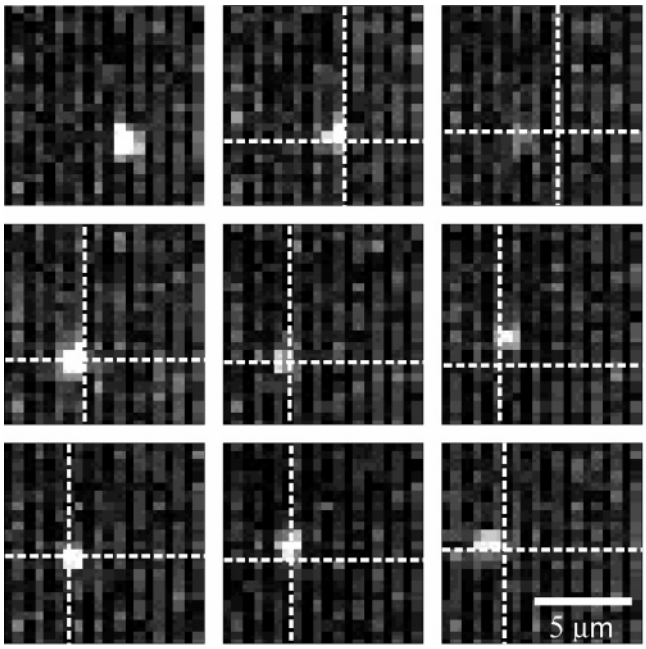

Figure 4. Sequential images revealing the motion of one nanotube in aqueous SDBS suspension. Each frame shows a 10 × 10 μm area and was acquired with a 50 ms exposure. Frames are sequenced from left to right starting at the top row. Dotted crossed lines mark the nanotube's position in the previous frame.

in Figure 3a and 3b, display a strong polarization dependence with no phase variation from one end to the other. By contrast, however, measurements of excitation polarization dependence for the curved object in Figure 3c reveal a phase shift of 25 ± 3° between the two ends, as plotted in Figure 4d. This shift matches the geometric angle of 25 ± 4° determined from the image of Figure 4c, confirming that the object is a bent nanotube with E_{22} optical absorption polarized strongly along the local tube axis. We have also measured emission spectra of selected regions within single nanotubes. The traces labeled #1 and #2 in Figure 4 show such spectra for opposite ends of the object in Figure 4b. The near-coincidence of these emission peaks clearly indicates that the entire nanotube has a consistent, well-defined (*n*,*m*) identity. However, there is a small spectral shift of ca. 2 meV between the two ends, which apparently reflects differences in local environment within the polymer host. For the bent nanotube of Figure 3c, we find a larger intratube spectral shift of approximately 4 meV (traces #3 and #4). The distinct spectra and polarization maxima observed for different segments within individual SWNT indicates an upper limit of a few micrometers on the distance that excitons can migrate within a nanotube during their lifetime.

It should be noted that the weakly sonicated samples also contained large nanotube bundles visible in bright-field microscopy. Emission from these objects was observable in our near-IR microscope, but with properties dramatically different from the individual nanotubes described above. First, emission from the bundles was completely insensitive to polarization of the excitation beam. Second, the bundles' emission spectra were broad and diffuse. We suggest that this emission arises from efficient light absorption followed by rapid nonradiative relaxation and consequent transient heating of the bundle and its surroundings to give nearly featureless thermal emission.

Near-infrared fluorescence microscopy also permits real-time tracking of nanotube motions in fluid media. Thin films of aqueous SWNT suspensions between fused silica slides were excited with laser powers near 400 W/cm^2 (~80 μm spot diameter) and the emission was imaged using our microscope and the prototype Roper OMA-V:2D near-IR camera. Nanotubes in fluids can be clearly imaged only if they remain relatively stationary during the exposure time needed to capture the image. With exposures of only 50 ms, our apparatus achieved signal-to-noise ratios near 5 for the most strongly fluorescing nanotubes. Figure 4 shows sequential 50 ms images of an individual nanotube as it is driven by Brownian motion and possibly convection caused by laser heating. Crosshairs drawn in each frame mark the nanotube's position in the preceding image. Analysis of these images reveals a mean square displacement (MSD) of 0.82 μm^2 per frame, which, using the relation $D = MSD/4\Delta t$, gives a diffusion coefficient of approximately 4 μm^2 s^{-1}. We note that this estimated diffusion coefficient is a factor of ~10 greater than the value reported for arc-grown SWNTs coated with biopolymers.[17] We interpret the changes in emission intensity as reorientation of the nanotube's axis relative to the polarization plane of the excitation laser. To our knowledge, fluorescence microscopy currently provides the only method capable of monitoring motions of pristine nanotubes on the sub-second time scale. We expect that higher excitation intensities will allow the time resolution of this method to be brought into the low millisecond range.

Conclusions. Near-infrared fluorescence microscopy is a useful new method for detecting and characterizing pristine semiconducting single-walled carbon nanotubes in a variety of media. When compared to established techniques such as AFM, STM, and SEM, fluorescence microscopy offers the advantages of relative experimental simplicity, rapid image acquisition through parallel detection, and versatility of sample environments. Although the method is limited to ca. 1 μm in spatial resolution and is not applicable to metallic, semi-metallic, or heavily derivatized SWNTs, it can be combined with emission spectroscopy to provide (*n*,*m*)-level identification of individual nanotubes. Alternatively, narrow-band optical filters can be added to generate (*n*,*m*)-selected images. The spectral properties of different segments within longer nanotubes can be studied to reveal inhomogeneous interactions of the nanotube with its environment and to check for spatial consistency of (*n*,*m*) structure. With time resolutions in the millisecond range, near-IR imaging will also permit kinetic studies of nanotube physical and chemical processes. Finally, SWNT fluorescence microscopy should find increasing use as a tool for noninvasively studying the interactions between nanotubes and biological systems.[18]

Acknowledgment. This research has been supported by the National Science Foundation (grant CHE-0314270), by the NSF Center for Biological and Environmental Nanotechnology (grant EEC-0118007), and by the Welch Foundation (grant C-0807). We are grateful to A. Guerra (Nikon)

and R. Guntupalli (Roper Scientific) for loans of equipment used in the course of this study and to the Rice Center for Nanoscale Science and Technology for instrumentation funding.

References

(1) Dresselhaus, M. S., Dresselhaus, G., Avouris, Ph., Eds. *Carbon Nanotubes: Synthesis, Structure, Properties, and Applications*; Springer-Verlag: New York, 2001; Vol. 80.
(2) Mews, A.; Koberling, F.; Basche, T.; Guenther, P.; Duesberg, G. S.; Roth, S.; Burghard, M. *Adv. Mater.* **2000**, *12*, 1210−1214.
(3) Hartschuh, A.; Sanches, E. J.; Xie, S. X.; Novotny, L. *Phys. Rev. Lett.* **2003**, *90*, 095503-1−4.
(4) Jiang, C.; Zhao, J.; Therese, H. A.; Friedrich, M.; Mews, A. *J. Phys. Chem.* **2003**, *107*, 8742−8745.
(5) Hadjiev, V. G.; Arepalli, S.; Nikolaev, P.; Jandl, S.; Yowell, L. *Nanotechnology* **2004**, *15*, 562−567.
(6) Chaudhary, S.; Kim, J. H.; Singh, K. V.; Ozkan, M. *Nano Lett.* **2004**, *4*, 2415−2419.
(7) Prakash, R.; Washburn, R.; Superfine, R.; Cheney, R.; Falvo, M. *Appl. Phys. Lett.* **2003**, *83*, 1219−1221.
(8) Otobe, K.; Nakao, H.; Hayashi, H.; Nihey, F.; Yudasaka, M.; Iijima, S. *Nano Lett.* **2002**, *2*, 1157−1160.
(9) O'Connell, M.; Bachilo, S. M.; Huffman, C. B.; Moore, V.; Strano, M. S.; Haroz, E.; Rialon, K.; Boul, P. J.; Noon, W. H.; Kittrell, C.; Ma, J.; Hauge, R. H.; Weisman, R. B.; Smalley, R. E. *Science* **2002**, *297*, 593−596.
(10) Bachilo, S. M.; Strano, M. S.; Kittrell, C.; Hauge, R. H.; Smalley, R. E.; Weisman, R. B. *Science* **2002**, *298*, 2361−2366.
(11) Hartschuh, A.; Pedrosa, H. N.; Novotny, L.; Krauss, T. D. *Science* **2003**, *301*, 1354−1356.
(12) Lefebvre, J.; Homma, Y.; Finnie, P. *Phys. Rev. Lett.* **2003**, *90*, 217401-1−4.
(13) Lefebvre, J.; Fraser, J. M.; Finnie, P.; Homma, Y. *Phys. Rev. B* **2004**, *69*, 075403-1−5.
(14) Lefebvre, J.; Fraser, J. M.; Homma, Y.; Finnie, P. *Appl. Phys. A* **2004**, *78*, 1107−1110.
(15) Htoon, H.; O'Connell, M. J.; Cox, P. J.; Doorn, S. K.; Klimov, V. I. *Phys. Rev. Lett.* **2004**, *93*, 027401-1−4.
(16) Paredes, J. I.; Burghard, M. *Langmuir* **2004**, *20*, 5149−5152.
(17) Lu, Q.; Freedman, O.; Rao, R.; Huang, G.; Lee, J.; Larcom, L. L.; Rao, A. M.; Ke, P. C. *J. Appl. Phys.* **2004**, *96*, 6722−6775.
(18) Cherukuri, P.; Bachilo, S. M.; Litovsky, S. H.; Weisman, R. B. *J. Am. Chem. Soc.* **2004**, *126*, 15638−15639.

NL050366F